

Chemical Science

Accepted Manuscript

This article can be cited before page numbers have been issued, to do this please use: Z. Di, Y. Qi, X. Yu, H. Li, M. Zuo, T. Ren, C. Li and Y. Zhao, *Chem. Sci.*, 2024, DOI: 10.1039/D4SC04619F.



This is an Accepted Manuscript, which has been through the Royal Society of Chemistry peer review process and has been accepted for publication.

Accepted Manuscripts are published online shortly after acceptance, before technical editing, formatting and proof reading. Using this free service, authors can make their results available to the community, in citable form, before we publish the edited article. We will replace this Accepted Manuscript with the edited and formatted Advance Article as soon as it is available.

You can find more information about Accepted Manuscripts in the [Information for Authors](#).

Please note that technical editing may introduce minor changes to the text and/or graphics, which may alter content. The journal's standard [Terms & Conditions](#) and the [Ethical guidelines](#) still apply. In no event shall the Royal Society of Chemistry be held responsible for any errors or omissions in this Accepted Manuscript or any consequences arising from the use of any information it contains.

Facile and scale-up syntheses of high-performance enzyme@meso-HOF biocatalysts

Zhengyi Di,^a Yu Qi,^a Xin-Xin Yu,^a Hai-Ruo Li,^a Meng-Xuan Zuo,^{a,b} Tian-Tian Ren,^a Cheng-Peng Li^{*a} and Yanli Zhao^{*b}

^aCollege of Chemistry, Tianjin Key Laboratory of Structure and Performance for Functional Molecules, Tianjin Normal University, Tianjin, 300387, China. E-mail: hxxylcp@tjnu.edu.cn

^bSchool of Chemistry, Chemical Engineering and Biotechnology, Nanyang Technological University, 21 Nanyang Link, 637371, Singapore. E-mail: zhaoyanli@ntu.edu.sg

Author contributions

Z.D. conceived the idea, designed the experiments, wrote the manuscript and provided financial support. Y.Q. and X.-X.Y. performed material synthesis and characterization. H.-R.L. helped with the material synthesis and data analysis. M.-X.Z. and T.-T.R. helped with the characterization and data analysis. C.-P.L. and Y.Z. supervised the experiments, wrote the manuscript and provided financial support.



ARTICLE

Facile and scale-up syntheses of high-performance enzyme@meso-HOF biocatalystsZhengyi Di,^a Yu Qi,^a Xin-Xin Yu,^a Hai-Ruo Li,^a Meng-Xuan Zuo,^{a,b} Tian-Tian Ren,^a Cheng-Peng Li^{*a} and Yanli Zhao^{*b}Received 00th January 20xx,
Accepted 00th January 20xx

DOI: 10.1039/x0xx00000x

Facile immobilization is essential for the wide application of enzymes in large-scale catalytic processes. However, exploration of suitable enzyme supports poses an unmet challenge, particularly in the context of scale-up biocatalyst fabrication. In this study, we present facile and scale-up syntheses of high-performance enzyme biocatalysts via in situ encapsulation of cytochrome c (Cyt-c) as mono-enzyme and glucose oxidase (GOx)-horseradish peroxidase (HRP) as dual-enzyme cascade (GOx&HRP) systems, respectively, into a stable mesoporous hydrogen-bonded organic framework (meso-HOF) matrix. In situ encapsulation reactions occur under ambient conditions, and facilitate scale up (~3 g/reaction) of enzyme@meso-HOF within a very short period (5–10 min). The resultant biocatalysts not only exhibit high enzyme loading (37.9 wt% for mono-enzyme and 22.8 wt% for dual-enzyme) with minimal leaching, but also demonstrate high catalytic activity, superior reusability, and durability. This study represents an example of scale-up fabrication of enzyme@meso-HOF biocatalysts in gram level and highlights the superior meso-HOFs as suitable host matrices for biomolecular entities.

Introduction

Enzymes, as biological catalysts, play critical roles in nearly all biochemical processes, exhibiting high specificity and activity to accelerate chemical reactions under ambient pressure and temperature.^{1–3} These attributes position enzymes as “core chip” in various scientific and industrial domains, including biotechnology,⁴ food industry,⁵ drug delivery,⁶ medical diagnostics,⁷ pharmaceutical industry,^{8, 9} and biofuels manufacturing.^{10, 11} The global enzyme market is projected to reach \$13.2 billion by 2027, with a compound annual growth rate of 8%.¹² However, the use of free enzymes presents challenges such as high cost, poor stability, and limited reusability.¹³ These obstacles impede the scaling up of free enzymes from laboratory or pilot-scale to industrial production levels.¹⁴ Immobilizing enzymes into/onto porous solid supports is considered an effective solution to address these challenges. Despite efforts to develop high-performance enzyme immobilization systems by adjusting matrices (e.g., organic polymers or inorganic metal oxides)^{15–18} and immobilization strategies (e.g., adsorption, covalent bonding, or crosslinking),^{19–21} current systems still face limitations, including difficulty in encapsulating large enzymes, inefficient substrate/product transfer due to nonporous carriers, and

enzyme denaturation and leaching.²² Therefore, expedited fabrication of high-performance immobilized biocatalysts on a large scale remains a pressing need.²³ In contrast to surface immobilization methods, in situ enzyme encapsulation strategy offers a versatile and effective approach by facilitating simultaneous self-assembly of enzymes and building units of the host matrix.²⁴ This approach aims to protect or stabilize enzymes within a specific environment, preserving their activity and functionality.²⁵ Notably, this strategy enables facile encapsulation of enzymes under mild conditions, such as aqueous phase, reasonable pH, and room temperature.¹² Furthermore, to enhance the contact rate between the reaction substrate and the loaded enzyme, the host matrix should possess high porosity and ordered open channels.²⁶

To date, crystalline porous solids such as metal-organic frameworks (MOFs),^{27–29} covalent-organic frameworks (COFs),^{30, 31} and hydrogen-bonded organic frameworks (HOFs)^{32, 33} have emerged as effective carriers for addressing the challenges of in situ enzyme encapsulation.³⁴ These materials offer tunable structures with easy functionalization and adjustable pore sizes within the mesoporous range.³⁵ Compared to MOFs and COFs that are constructed from metal coordination and covalent bonding interactions, HOFs are assembled through weak hydrogen-bonding contacts aided by rich π - π stacking interactions.^{36–38} This approach endows HOFs with highly dynamic and flexible structures.^{39–41} The metal-free nature of HOFs provides better biocompatibility and lower toxicity, making them highly desirable for biocatalyst and biomedicine applications. Furthermore, HOFs can self-assemble in solutions at ambient temperature, allowing enzymes to be immobilized without degradation.⁴² Despite the reported success of some HOF-based bio-immobilization matrices, there

^a College of Chemistry, Tianjin Key Laboratory of Structure and Performance for Functional Molecules, Tianjin Normal University, Tianjin, 300387, China. E-mail: hxxylcp@tjnu.edu.cn

^b School of Chemistry, Chemical Engineering and Biotechnology, Nanyang Technological University, 21 Nanyang Link, 637371, Singapore. E-mail: zhaoyanli@ntu.edu.sg

† Electronic Supplementary Information (ESI) available: experimental details and supplementary figures and tables. See DOI: 10.1039/x0xx00000x



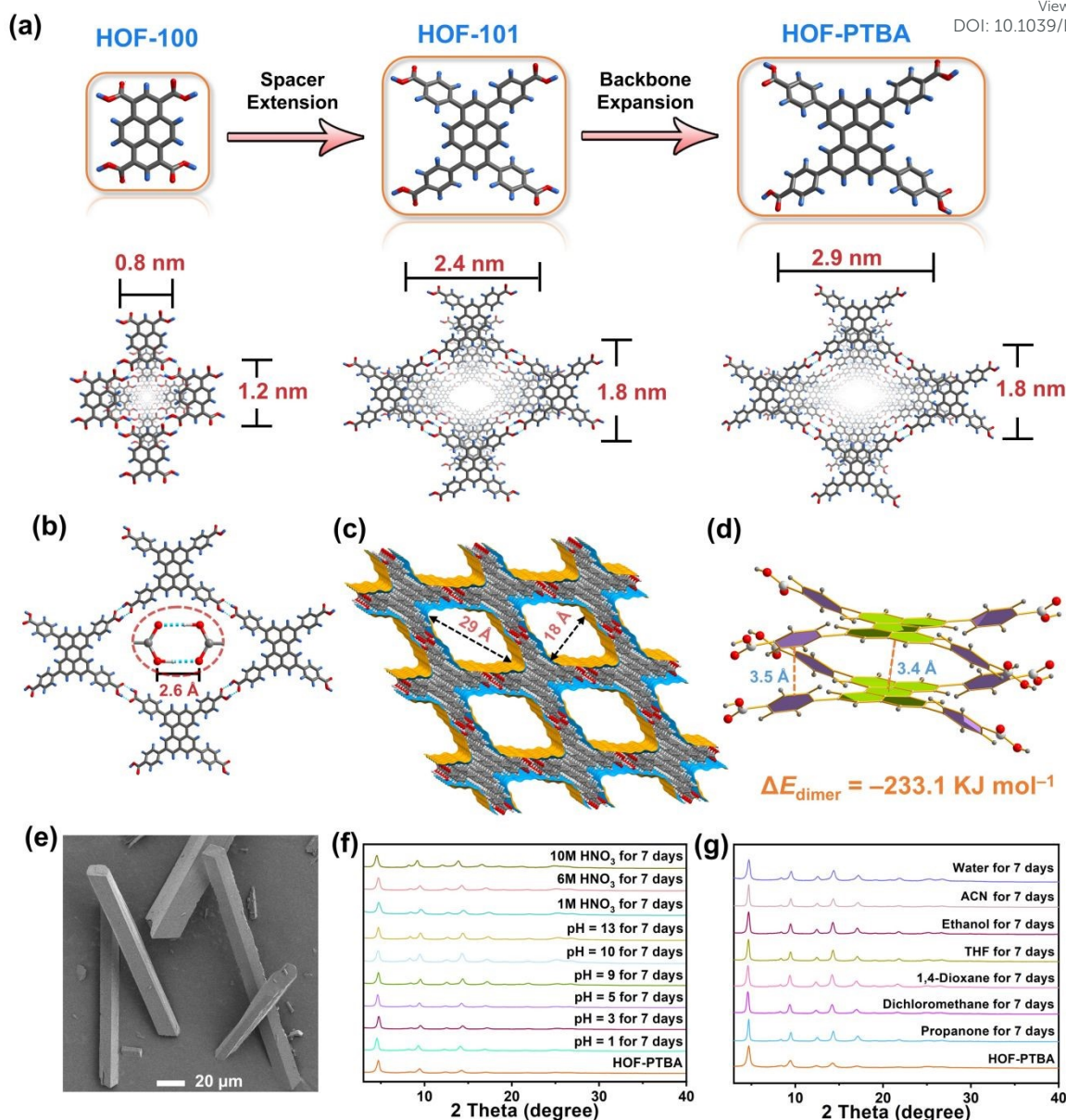


Figure 1. a) Fabrication strategy of HOF-PTBA by backbone expansion approach. b) 2D H-bonding layer in HOF-PTBA, highlighting the O–H...O bonds. c) 1D channels (18 × 29 Å) in HOF-PTBA. d) Face-to-face π – π interactions (interlayer distance 3.4 and 3.5 Å) in HOF-PTBA. e) SEM image of HOF-PTBA. f) PXRD patterns for structural stability of HOF-PTBA under various pH conditions for 7 days. g) PXRD patterns of HOF-PTBA with different solutions for 7 days.

is still a pending trade-off between increasing the open aperture size and improving the stability of HOFs.^{43, 44} Specifically, achieving a combination of large pore size and high stability within a single HOF material remains an unmet challenge.^{45–47}

The ligand modification and extension approach have been widely used in the design of MOFs and COFs to fabricate mesoporous solids.^{48–53} This sophisticated approach involves extending ligands or monomers by introducing enlarged linkers between reactive groups, albeit with the inherent risk of network interpenetration.^{54, 55} Notably, this strategy has also been applied to design a series of stable two-dimensional (2D)

HOFs, known as HOF-10x (x = 0,1,2).⁵⁶ By incorporating benzene and naphthalene spacers between perylene and carboxyl groups in the HOF-10x monomers, the channel sizes exhibit a systematic increase from HOF-100 to HOF-101 and HOF-102. However, increasing the length of HOF monomers may lead to undesirable network interpenetration or layer staggering arrangements, resulting in decreased pore size and compromised stability.^{39, 57, 58} With these in mind, we propose that HOF monomers with bulky fused aromatic rings could effectively address the trade-off between porosity and stability within a single HOF. Specifically, expanding the backbone of the conjugated system in HOFs is anticipated to enhance pore size



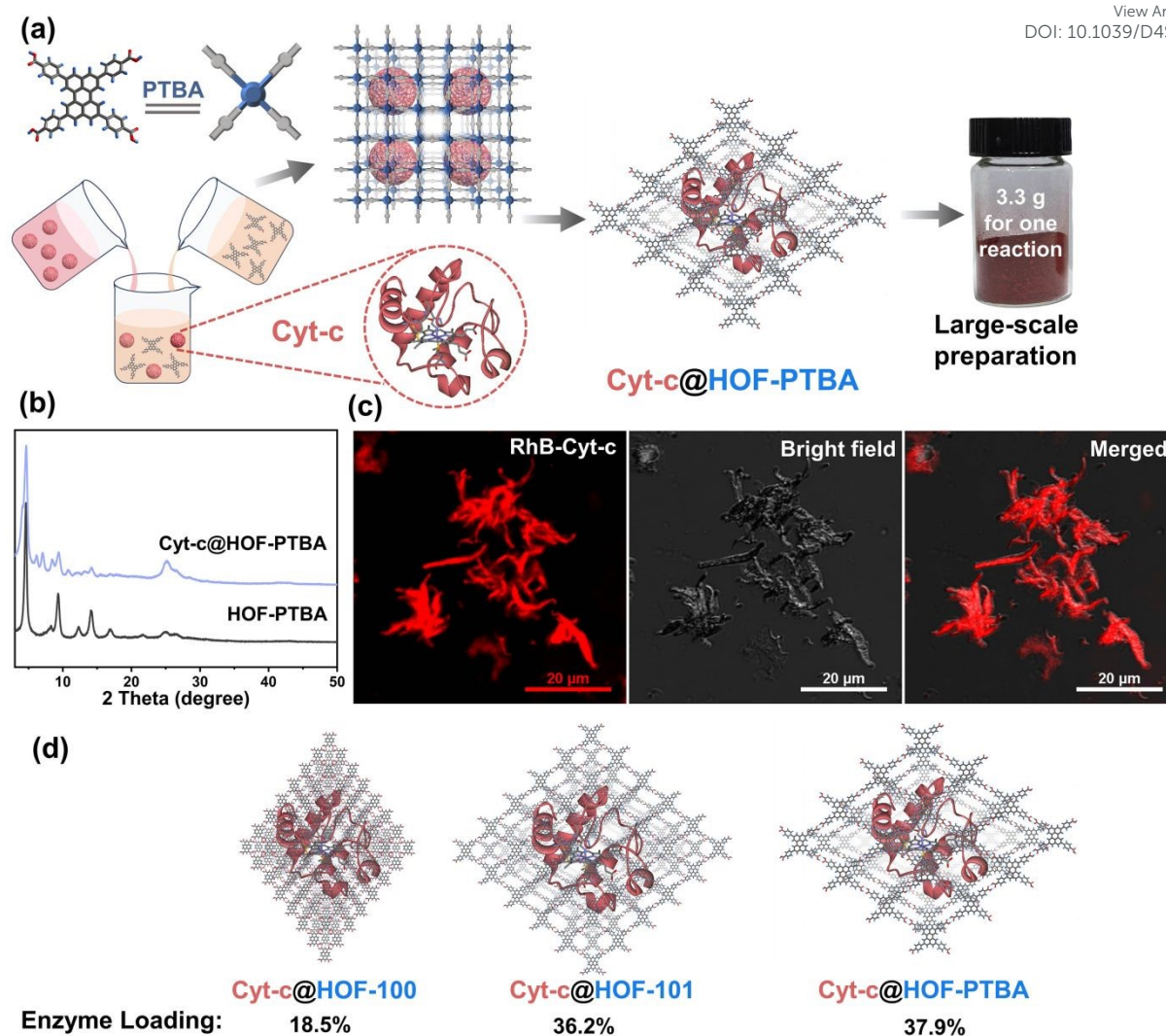


Figure 2. a) Facile synthesis of Cyt-c@HOF-PTBA at room temperature and digital photograph based on a scale-up synthesis (3.3 g for one reaction). b) PXRD patterns of Cyt-c@HOF-PTBA and HOF-PTBA. c) CLSM images of Cyt-c@HOF-PTBA (Cyt-c was labelled by red dye). d) Calculated Cyt-c loadings by different HOFs supported by the ICP-MS measurements.

while promoting more stable π - π interactions between the eclipsed 2D layers simultaneously.

To validate this hypothesis, we are motivated by using a bulky π -conjugation system of perylene as the backbone of HOF monomer to construct ultrastable mesoporous HOF-PTBA (Figure 1a), serving as a host matrix for in situ encapsulation of enzymes. HOF-PTBA can be readily scaled up for preparation under mild conditions (aqueous solution and room temperature). It features a one-dimensional (1D) square channel measuring $18 \times 29 \text{ \AA}$ and remains stable in various environments, including water, organic solvent, 10 M HNO_3 and 0.1 M NaOH for at least 7 days. These features enable us to develop an enzyme immobilization scaffold for fabricating enzyme@meso-HOF biocatalysts. To assess the universality of this approach, we select cytochrome c (Cyt c) as mono-enzyme and glucose oxidase (GOx)-horseradish peroxidase (HRP) as dual-enzyme cascade (GOx&HRP) systems, and confine them

within HOF-PTBA mesoporous environments. Notably, in situ encapsulation reactions occur under ambient conditions, and facilitate scale up ($\sim 3 \text{ g/reaction}$) of enzyme@HOF within a very short period (5–10 minutes). The resulting enzyme@HOF materials demonstrate high enzyme loading with minimal leaching, high catalytic activity, and superior reusability and durability. This study represents a pioneer example for the scale-up fabrication of enzyme@HOF biocatalysts, and highlights the meso-HOFs as host matrices for biomolecular entities.

Results and Discussion

To address the trade-off effect between stability and porosity of crystalline frameworks, we design and fabricate a mesoporous HOF with the pore size of $18 \times 29 \text{ \AA}$ by employing a novel backbone extension strategy (Figure 1a). This strategy



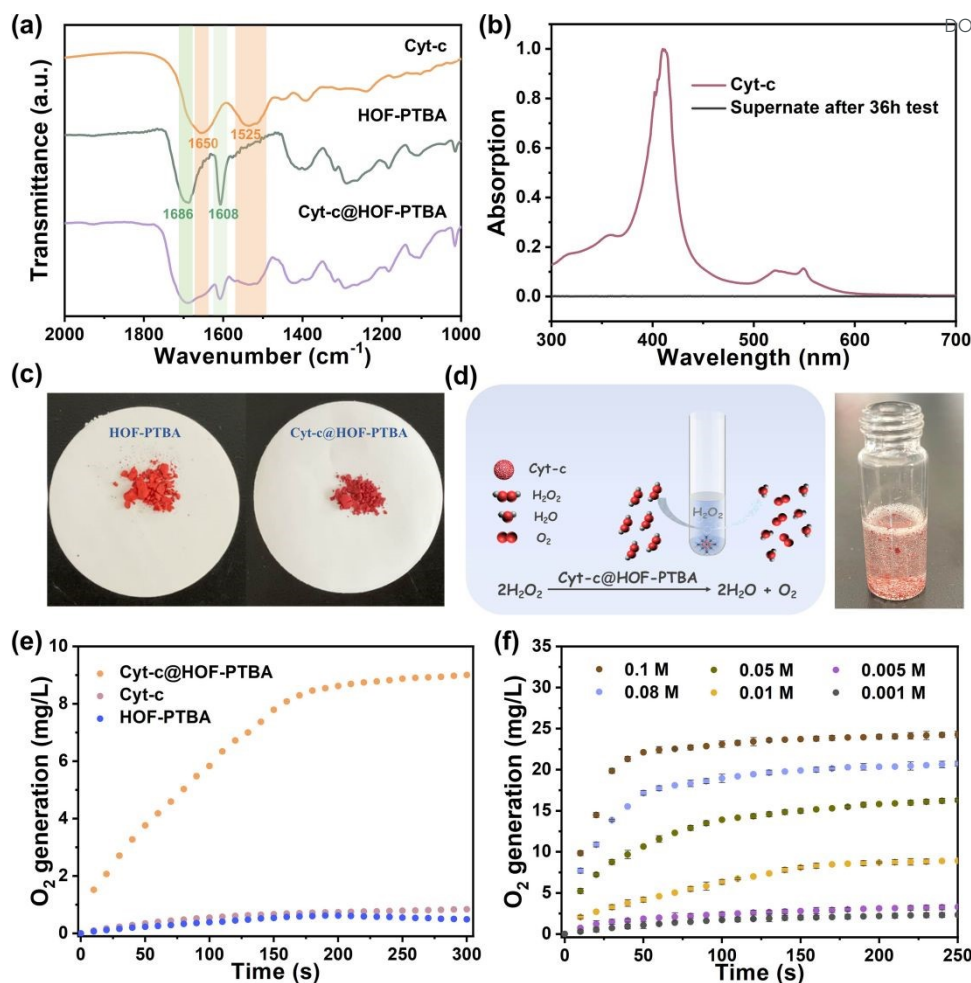


Figure 3. a) FT-IR spectra of HOF-PTBA, Cyt-c@HOF-PTBA, and Cyt-c. b) UV-vis spectra of the collected supernatants after biomimetic mineralization process. c) Color comparison between HOF-PTBA and Cyt-c@HOF-PTBA. d) Catalytic reaction and digital photograph showing the O₂ bubble generation using Cyt-c@HOF-PTBA catalyst. e) Capacity of O₂ generation via H₂O₂ decomposition by Cyt-c@HOF-PTBA, Cyt-c and HOF-PTBA. f) H₂O₂-dependent catalytic kinetic curves of Cyt-c@HOF-PTBA catalyst. All tests were carried out at Tris buffer (pH 7.5, 50 mM). Cyt c dosage was kept at 0.1 mg/mL.

offers several advantages: Firstly, the introduction of matrices with larger π -conjugation creates HOFs with higher porosity. Secondly, bulky aromatic building units of HOFs enhance the interactions between the H-bonded 2D layers. Thirdly, the ordered and porous channels in HOFs would increase the transport rate of substrates, thereby improving the efficiency of enzyme catalysis. Additionally, the crystal structure can be obtained through single-crystal X-ray diffraction measurements, which facilitates the determination of the spatial positions of the atoms and provides a theoretical basis for the design and synthesis of more stable HOF structures.

The 1,3,6,8-tetrakis(benzoic acid)perylene (H₄PTBA) organic building block was obtained from a 3-step synthesis, as illustrated in Figure S1, and confirmed by ¹H NMR (Figures S2–S4). The molecular structures of HOF-100, HOF-101 and HOF-PTBA were shown at Figure S5. High-quality single crystals of HOF-PTBA were synthesized by slow vapor diffusion from DMF-

MeOH medium at room temperature (Figure S6). Single-crystal X-ray diffraction studies revealed that HOF-PTBA crystallizes in monoclinic space group *C2/m* (Table S1). The asymmetric unit of HOF-PTBA contains a quarter H₄PTBA molecule, which remains undeprotonated (Figure S7). Each H₄PTBA molecule interacts with four neighbouring molecules through eight O–H...O hydrogen bonds, extending into a 2D layer. The O–H...O distance measures 2.6 Å (Figures 1b and S8), falling within the strong hydrogen bond range. Each 2D square layer interacts with adjacent layers through face-to-face π – π stacking interactions (interlayer distance 3.4 Å) to form a 1D square channel of 18 × 29 Å (Figures 1c and S9–S11). The permanent porosity of HOF-PTBA was disclosed by N₂ sorption measurement at 77 K, which shows that HOF-PTBA possesses the typical type IV sorption profile, indicating its mesoporous nature (Figure S12). The pore size distribution profiles derived



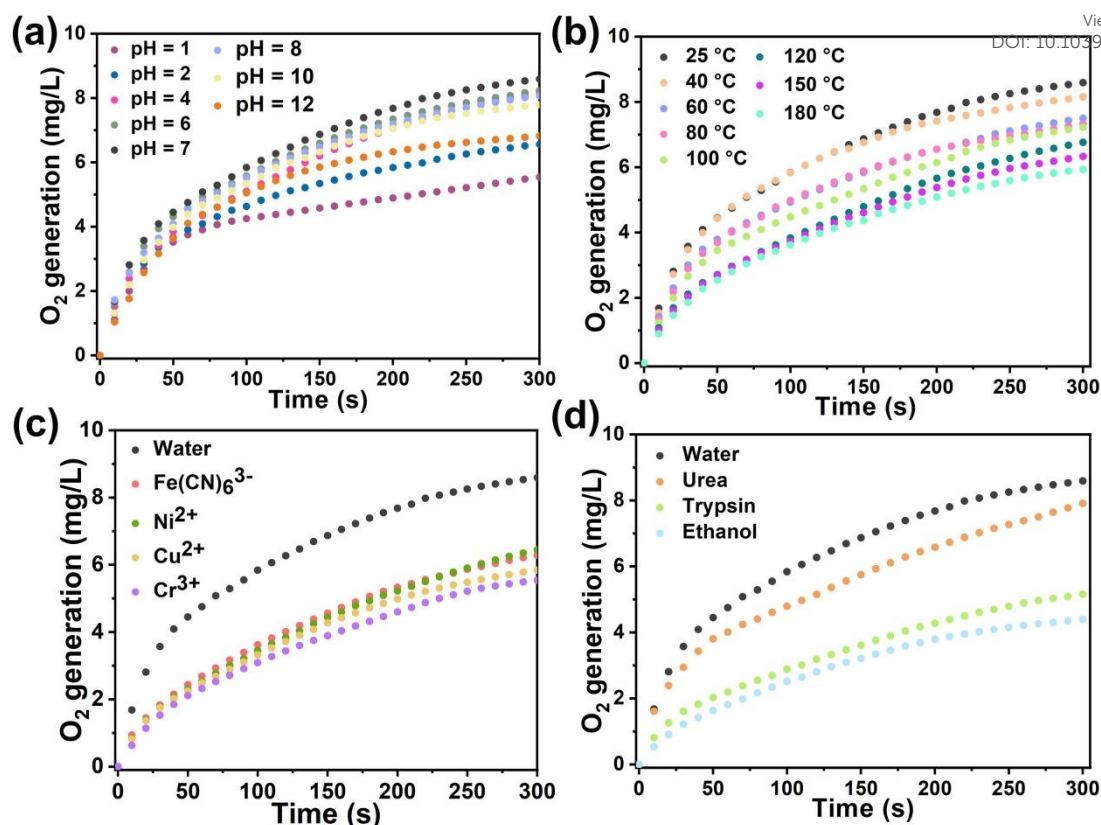


Figure 4. Catalytic kinetics of Cyt-c@HOF-PTBA after treatment by non-physiological pH (a), heating for 30 min (b), heavy metal ions (c), denaturing reagents and organic solvents (d).

from these isotherms were centered at about 2.3 nm (Figure S13).

As depicted in Figures 1d and S14, the bulky π -conjugated perylene groups in HOF-PTBA are stacked in an AA arrangement, significantly increasing the aromatic stacking energy. The energy for HOF-PTBA dimer is $-233.1 \text{ kJ mol}^{-1}$, which is much higher than hydrogen bonding energy of $-46.6 \text{ kJ mol}^{-1}$, demonstrating the vital role of π - π stacking for structural stability. In comparison, the energy for PFC-1 dimer is $-199.8 \text{ kJ mol}^{-1}$, with the hydrogen bonding energy of $-47.1 \text{ kJ mol}^{-1}$. Consequently, HOF-PTBA exhibits stronger π -conjugated interactions and thus a more stable structure than PFC-1. Meanwhile, the peaks of PTBA at 1418 and 1290 cm^{-1} were found to be red-shifted to 1409 and 1285 cm^{-1} in HOF-PTBA from the FT-IR spectra, indicating the presence of π - π stacking interactions (Figure S15).⁵²

The as-synthesized (Figure 1e) and scale-up products of HOF-PTBA are nearly identical, as determined by powder X-ray diffraction (PXRD) (Figure S16). Even after being soaked in 1 M, 6 M and 10 M HNO_3 aqueous solutions for 7 days, HOF-PTBA maintains its crystallinity well. Remarkably, HOF-PTBA retains its crystallinity even under strong alkaline conditions at $\text{pH} = 13$ for 7 days, a rarity for carboxyl-HOFs (Figure 1f). For comparison, PFC-1 is only stable for 14 hours at $\text{pH} = 13$, providing the basis for the HOF-PTBA to be used in more harsh environments. Furthermore, HOF-PTBA remains intact in different solvents for tetrahydrofuran (THF), 1,4-dioxane, dichloromethane, and

propanone (Figure 1g). Even after 545 days of immersion in various solvents, HOF-PTBA still maintained good crystallinity (Figure S17). The thermal stability of HOF-PTBA was 7 days, including water, acetonitrile (ACN), ethanol, confirmed by thermogravimetric analysis (TGA), showing that the framework remains unchanged up to $440 \text{ }^\circ\text{C}$ (Figure S18). Therefore, the excellent solvent stability, acid and alkali resistance, and thermal stability of HOF-PTBA make it a potential support for enzyme immobilization.

To demonstrate the feasibility of HOF-PTBA for enzyme loading, we chose Cyt-c as a representative biocatalyst. Encapsulation of Cyt-c into HOF-PTBA was achieved through a biomimetic mineralization process. The enzyme solution was added to the solution containing the H_4PTBA monomer by a simple one-pot method (Figure 2a). After stirring for about 5 minutes at room temperature, the biocomposite (named Cyt-c@HOF-PTBA) was isolated in gram level ($\sim 3.3 \text{ g/reaction}$). The weight loss of Cyt-c@HOF-PTBA in the range of 290 – $440 \text{ }^\circ\text{C}$ in the TG curves was caused by the pyrolysis of the incorporated Cyt-c (Figure S18). As depicted in Figure 2b, the framework of HOF-PTBA remains unchanged after enzyme immobilization, as revealed by PXRD. The distribution of Cyt-c in Cyt-c@HOF-PTBA was characterized by confocal laser scanning microscopy (CLSM) experiments, wherein Cyt-c was labelled with rhodamine B (RhB), a red fluorescent dye.²⁶ The red fluorescence completely covered the material (Figure 2c), suggesting uniform spatial distribution of Cyt-c. According to the results from CLSM, the



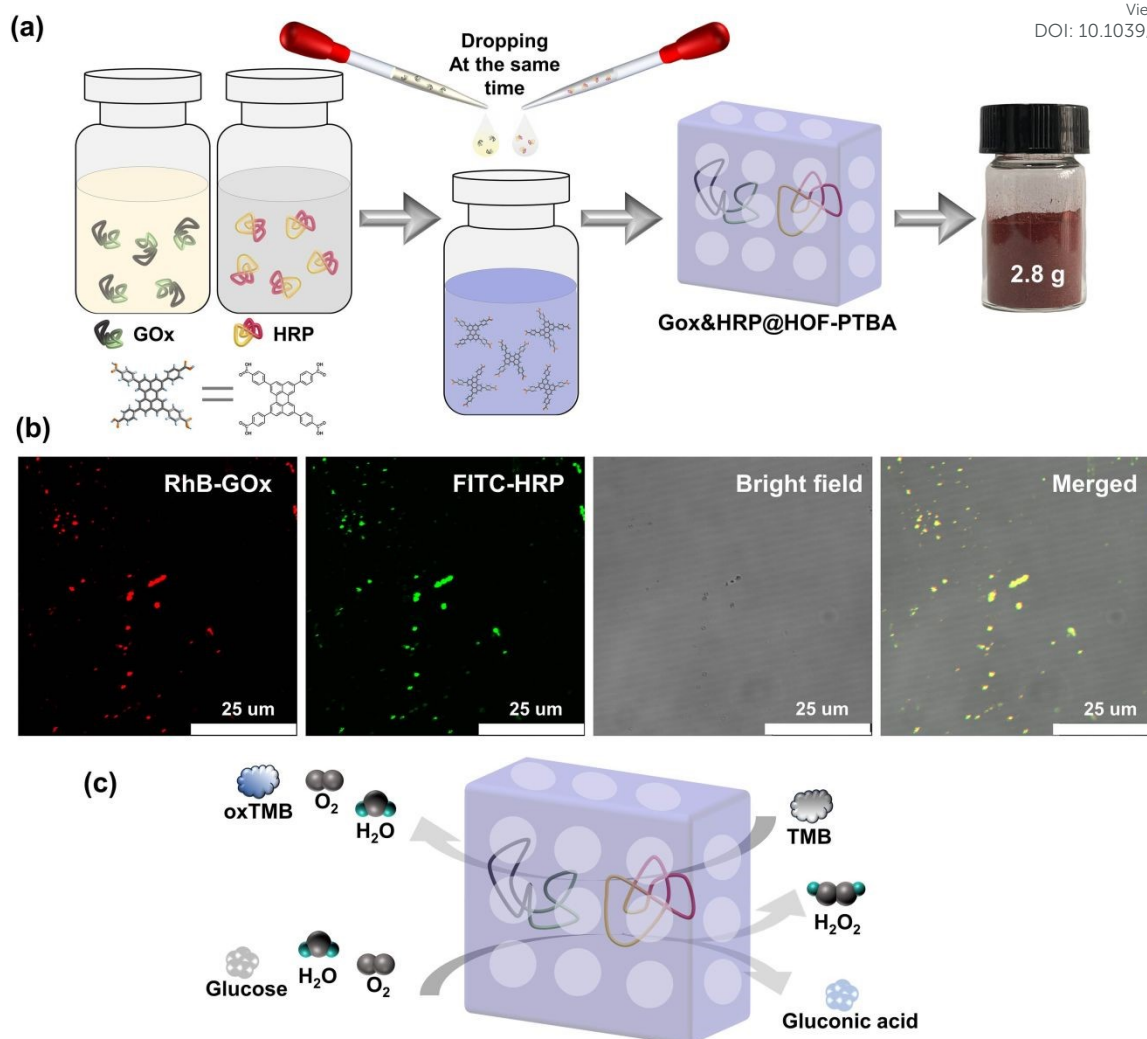


Figure 5. a) Facile synthesis of GOx&HRP@HOF-PTBA at room temperature and digital photograph based on a scale-up synthesis (2.8 g for one reaction). b) CLSM images of GOx&HRP@HOF-PTBA (GOx was labelled with red dye and HRP was labelled with green dye). c) Cascade reaction mechanism using GOx&HRP@HOF-PTBA as the catalyst.

enzymes were evenly distributed throughout the entire structure of HOF, rather than located inside the pores.^{59–61} The standard Bradford assay (Figure S19) indicated a Cyt-c content of 40.8 wt% in the nanosystem. Such a high enzyme loading was also confirmed by inductively coupled plasma-mass spectra (ICP-MS) (Figure S20), wherein Cyt-c was calculated on average to be 37.9 wt% in Cyt-c@HOF-PTBA (Table S2). This value exceeded that of HOF-100 (18.5 wt%) and HOF-101 (36.2 wt%) (Figure 2d). These results clearly confirmed the successful encapsulation of Cyt-c within the pores of HOF-PTBA to form the Cyt-c@HOF-PTBA biocomposite.

To verify the stability of the encapsulated material, we soaked 1.5 mg of Cyt-c@HOF-PTBA in 5 mL of aqueous solution for 36 h. As shown in Figure 3a, the FT-IR spectrum of Cyt-c@HOF-PTBA revealed the presence of amide I (1650 cm^{-1}) and amide II (1525 cm^{-1}) bands of Cyt-c,⁶² indicating that Cyt-c remained encapsulated in the HOF. To accurately determine the interfacial interactions between Cyt-c and the host HOF matrix, the solid-state NMR (ssNMR) spectroscopy was employed.^{63, 64}

As a result, the ssNMR spectra of Cyt-c@HOF-PTBA were obviously different from those of the free enzyme and the physical mixture of enzyme and HOF (Figure S21). In the ^1H and ^{13}C ssNMR spectra of HOF-PTBA, the chemical shifts of the carboxyl group were in the ranges of 19–20 ppm and 164–165 ppm respectively, which were found to be shifted in Cyt-c@HOF-PTBA. Thus, additional interactions between Cyt-c and HOF-PTBA facilitate the enzyme immobilization.⁶² Moreover, no absorption peak was observed in the UV-vis curve of the supernatant after 36 h biomimetic mineralization process, showing no leaching of Cyt-c after treatment (Figure 3b). Notably, the color of materials darkened after immobilization, attributed to Cyt-c being encapsulated within the framework of HOF-PTBA (Figure 3c).

The coordination environments of heme in both free Cyt-c and Cyt-c@HOF-PTBA were examined using electron paramagnetic resonance (EPR) spectroscopy. The results revealed that both forms contained high-spin ferric heme with g-values of 5.97 and 5.68 (Figure S22). However, no low-spin



ferric heme signal ($g = 2.93$ and 2.29) was detected in Cyt-c@HOF-PTBA, as observed in previous studies.^{65, 66} These results indicate that encapsulation within HOF-PTBA alters the conformation of Cyt-c, leading to the observed catalase-like biocatalytic properties in Cyt-c@HOF-PTBA.

To assess the feasibility of enzyme encapsulation, we evaluated the biocatalytic performance of Cyt-c@HOF-PTBA (Figure 3d). Interestingly, Cyt-c@HOF-PTBA exhibited catalase-like bioactivity, decomposing H_2O_2 into O_2 and H_2O (Figures 3e and S23).⁶² Figure 3f illustrates that the catalytic activity of Cyt-c@HOF-PTBA was dependent on substrate concentration (0.001–0.1 M), with higher concentrations yielding greater activity. Specifically, at an H_2O_2 concentration of 0.1 M, the oxygen yield in the presence of Cyt-c@HOF-PTBA reached 22.1 mg/L in 50 seconds, representing a 1.95-fold increase in catalytic rate compared to Cyt-c@HOF-101 (Table S3).⁶² To further evaluate the catalytic activities of Cyt-c encapsulated by HOF-PTBA and HOF-101, Michaelis-Menten model was employed (see Supporting Information for details). As a result, the Michaelis constant K_m of Cyt-c@HOF-PTBA is 29.7 mM/s, being lower than that of Cyt-c@HOF-101 (32.3 mM/s), which indicates that the binding interactions between the enzyme and the substrate in Cyt-c@HOF-PTBA are stronger (Figure S24 and Table S4). These findings indicate that a larger pore structure enhances the catalytic efficiency of the loaded enzyme.

In general, biological enzyme catalysts are costly and difficult to recover, and their catalytic activity is sensitive to external environments such as temperature and pH (Figure S25). Immobilizing enzymes within HOF pores may mitigate these issues and advance enzyme development in industry. We assessed the catalytic kinetics of the composites by subjecting Cyt-c@HOF-PTBA to various pH solutions for 30 minutes at room temperature. As a result, the biocomposite maintained efficient H_2O_2 catalytic activity over a wide pH range from acidic (pH = 1) to basic (pH = 12) conditions (Figure 4a). At pH = 2, Cyt-c@HOF-PTBA exhibited 1.61 times higher catalytic activity than Cyt-c@HOF-101. Even at pH = 12, Cyt-c@HOF-PTBA still retained 80% catalytic activity, owing to extensive π -conjugation system of HOF-PTBA to provide effective protection for Cyt-c under extreme pH conditions. Temperature significantly impacts enzyme catalysis activity, often leading to deactivation at high temperatures, thus requiring storage at low temperatures. We subjected Cyt-c@HOF-PTBA to temperatures ranging from 25 to 180 °C for 30 minutes (Figure 4b), and evaluated its H_2O_2 catalytic ability. Remarkably, catalytic activity remained relatively stable up to 40 °C (activity: 95%). Even at 100 °C, catalysis activity was sustained at 87%. Notably, under 180 °C, catalytic activity remained high (activity: 69%), enabling enzyme catalyst usage in extreme temperature environments. In addition, we assessed the protective effect of HOF-PTBA against harsh conditions, including heavy metal ions and denaturing reagents. As depicted in Figure 4c, Cyt-c@HOF-PTBA retained at least 65% activity in the presence of $Fe(CN)_6^{3+}$, Ni^{2+} , Cu^{2+} , and Cr^{3+} . Moreover, Cyt-c@HOF-PTBA exhibited robust resistance to urea, maintaining 92% catalysis activity (Figure 4d).

The exceptional stability of Cyt-c@HOF-PTBA prompted us to assess its duration without additional protection, which could

offer significant advantages in storage and transportation (Figure S26). We conducted an evaluation by incubating Cyt-c@HOF-PTBA at 35 °C for 1–8 days and subsequently testing its catalytic activity. Remarkably, experimental results revealed that HOF-PTBA maintained 72% catalytic activity even after 8 days (Figure S27). These results encouraged us to explore the reusability of Cyt-c@HOF-PTBA biocatalyst, aiming to reduce overall costs and facilitate industrial catalysis. The catalytic ability of Cyt-c@HOF-PTBA remained nearly unchanged after five cycles, retaining 71% of its original activity even after 10 cycles (Figure S28). The slight decrease in catalytic activity during the recycling assay may be due to the loss of Cyt-c@HOF-PTBA during centrifugation and filtration steps. These results underscore the remarkable attributes of Cyt-c@HOF-PTBA, including high catalytic activity, durability, reusability, and resistance to harsh environments. Thus, HOF-PTBA represents an ideal model for enzyme immobilization, highly desirable for long-term applications in enzyme catalysis.

Encouraged by the results, we proceeded to assess the universality of immobilization supports and extended it to the encapsulation of multiple enzymes. Multienzymes biocatalytic cascade (MBC) play crucial roles in living organisms, serving functions such as signal transmission and metabolic pathways within cells.⁶⁷ Immobilizing multiple enzymes within the same framework can emulate cell-like spatial isolation,⁶⁸ simulating complex cellular environments with sequential intercommunication and instant signal feedback, thereby enabling specific organism functions. The large pore structure of mesoporous HOF-PTBA facilitates the transport of catalytic substrates, allowing us to achieve a biocatalytic cascade reaction by loading GOx and HRP. In situ encapsulation dual-enzyme GOx and HRP within HOF-PTBA can be easily obtained by mixing and stirring them at ambient conditions for 5 minutes, resulting in the production of 2.8 g GOx&HRP@HOF-PTBA biocatalysts through centrifugation (Figure 5a). As shown in the CLSM images (Figure 5b), the encapsulated GOx and HRP enzymes were uniformly distributed in the composites, with GOx and HRP labelled with RhB and fluorescein isothiocyanate (FITC), respectively. The PXRD patterns showed similar peaks between GOx&HRP@HOF-PTBA and HOF-PTBA (Figure S29), indicating the intact of crystalline mesoporous framework during the immobilization reactions. In the FT-IR spectra (Figure S30), the presence of similar amide I peaks at 1700–1610 cm^{-1} and amide II peaks at 1590–1485 cm^{-1} in GOx&HRP@HOF-PTBA confirms the successful encapsulation of GOx and HRP within HOF-PTBA. The enzyme loadings of GOx and HRP in biocomposite were determined to be 11.3% and 11.5% based on ICP-MS method (Table S5), respectively. The loading amounts of GOx and HRP in the biocomposite were also quantitatively confirmed by fluorescence changes of the supernatant before and after encapsulation (Figures S31–S34), giving values of 11.2% and 11.9%, respectively (Table S6). After soaking GOx&HRP@HOF-PTBA in buffer solution for 10 days, no enzyme leaching was observed in the solution (Figure S35). TGA curve of GOx&HRP@HOF-PTBA indicated that the pyrolysis of dual-enzyme occurred around 250–450 °C (Figure S36).



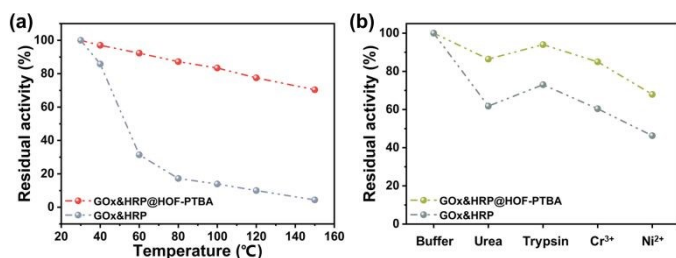


Figure 6. Residual activity of GOx&HRP@HOF-PTBA after treatment by heating for 30 min (a), denaturing reagents and heavy metal ions (b).

We further investigated the biocatalytic cascade performance of GOx&HRP@HOF-PTBA. The dual-enzyme cascade reactions involve the oxidation of glucose solution in the presence of GOx, yielding H₂O₂ and gluconic acid, with H₂O₂ subsequently acting as a substrate for HRP to catalyze the oxidation of TMB to oxidized TMB (oxTMB) (Figure 5c). The quantity of blue oxTMB products can be evaluated using UV-Vis spectroscopy (Figure S37). We assessed the feasibility of in situ encapsulation of the dual enzymes by comparing the catalytic activity of GOx&HRP@HOF-PTBA with that of GOx&HRP mixture under different temperature conditions, pH levels, metal ions, and denaturing reagents. Compared to free GOx&HRP, GOx&HRP@HOF-PTBA exhibited notable advantages in residual activity with increasing reaction temperatures (Figure 6a), the higher the temperature is, the bigger the gap is. When the reaction temperature is over 80 °C, the residual activity of GOx&HRP mixture was lower than 20%, meanwhile that of GOx&HRP@HOF-PTBA was still close to 90% (Figure S38). Regarding pH effects, GOx&HRP@HOF-PTBA demonstrated higher residual activity at acidic (pH = 2) and neutral (pH = 7) conditions (Figure S39). In the presence of deactivating reagents, such as urea, trypsin, Cr³⁺ and Ni²⁺, the enzyme activity of GOx&HRP@HOF-PTBA was significantly higher (21%–25%) than that of free GOx&HRP, because of the rigid encapsulation support of HOF-PTBA (Figures 6b and S40). In addition, the performance of GOx&HRP@HOF-PTBA surpassed that of free GOx&HRP in organic solvent environments (Figures 41 and S42). Long-term storage stability at room temperature was evaluated by measuring residual activities daily (Figure S43). While the activity of free GOx&HRP decreased considerably and remained only 24% after 12 days, GOx&HRP@HOF-PTBA retained approximately 61% of its initial activity after 12 days (Figure S44). These results clearly demonstrate that GOx&HRP@HOF-PTBA possesses enhanced stability and higher duration, validating the advantages of the in-situ encapsulation strategy.

Conclusion

In summary, we have presented a facile and versatile enzyme encapsulation strategy for scaling up high-performance enzyme@meso-HOF biocatalysts. The ultrastable mesoporous HOF-PTBA was fabricated by selecting building units with larger conjugated π -systems, which could remain intact even in harsh conditions such as 10 M HNO₃ and pH = 13. Furthermore, HOF-

PTBA could effectively protect mono- and dual-enzymes during the initial growth phase, enabling the retention of biocatalytic activity after encapsulation. Enzymes confined within the ordered and robust HOF-PTBA network exhibited enhanced stability and maintained their biological activity even after exposure to harsh treatments, including heating, organic solvents, metal ions, denaturing reagents, and acid-base solutions. Significantly, the scaled-up syntheses of biocatalysts can be conveniently achieved under mild conditions (aqueous solution and room temperature), aligning perfectly with the principles of green and environmentally friendly production. This study not only overcomes the key bottleneck of current enzyme immobilization technology, but also paves the way for the preparation of high-performance biocatalysts and offers a platform for enzyme industrialization.

Author contributions

Z.D. conceived the idea, designed the experiments, wrote the manuscript and provided financial support. Y.Q. and X.-X.Y. performed material synthesis and characterization. H.-R. Li helped with the material synthesis, data analysis. M.-X.Z. and T.-T.R. helped with the characterization and data analysis. C.-P.L. and Y.Z. supervised the experiments, wrote the manuscript and provided financial support.

Conflicts of interest

There are no conflicts to declare.

Acknowledgements

We acknowledge the financial supports of the National Nature Science Foundation of China (22171210 and 22205163) and the National Research Foundation Singapore under Its Competitive Research Programme (NRF-CRP26-2021-0002). We thank Dr. Yu-Xia Wang (Tianjin Normal University) for the EPR measurements and analysis.

Notes and references

- Q. Zhu, Y. Zheng, Z. Zhang and Y. Chen, *Nat. Protoc.*, 2023, **18**, 3080–3125.
- C. Doonan, R. Ricco, K. Liang, D. Bradshaw and P. Falcaro, *Acc. Chem. Res.*, 2017, **50**, 1423–1432.
- Q. Sun, Y. Pan, X. Wang, H. Li, J. Farmakes, B. Aguila, Z. Yang and S. Ma, *Chem*, 2019, **5**, 3184–3195.
- U. T. Bornscheuer, G. W. Huisman, R. J. Kazlauskas, S. Lutz, J. C. Moore and K. Robins, *Nature*, 2012, **485**, 185–194.
- A. S. Meyer, *Ann. N. Y. Acad. Sci.*, 2010, **1190**, 126–132.
- H. Zheng, Y. Zhang, L. Liu, W. Wan, P. Guo, A. M. Nyström and X. Zou, *J. Am. Chem. Soc.*, 2016, **138**, 962–968.
- J. Zhuang, C.-H. Kuo, L.-Y. Chou, D.-Y. Liu, E. Weerapana and C.-K. Tsung, *ACS Nano*, 2014, **8**, 2812–2819.
- P. Horcajada, R. Gref, T. Baati, P. K. Allan, G. Maurin, P. Couvreur, G. Férey, R. E. Morris and C. Serre, *Chem. Rev.*, 2011, **112**, 1232–1268.



9. S. Wu, R. Snajdrova, J. C. Moore, K. Baldenius and U. T. Bornscheuer, *Angew. Chem. Int. Ed.*, 2020, **60**, 88–119.
10. D. Feng, T.-F. Liu, J. Su, M. Bosch, Z. Wei, W. Wan, D. Yuan, Y.-P. Chen, X. Wang, K. Wang, X. Lian, Z.-Y. Gu, J. Park, X. Zou and H.-C. Zhou, *Nat. Commun.*, 2015, **6**, 5979.
11. S. J. Cobb, A. M. Dharani, A. R. Oliveira, I. A. C. Pereira and E. Reisner, *Angew. Chem. Int. Ed.*, 2023, **62**, e202218782.
12. Y. Zheng, S. Zhang, J. Guo, R. Shi, J. Yu, K. Li, N. Li, Z. Zhang and Y. Chen, *Angew. Chem. Int. Ed.*, 2022, **61**, e202208744.
13. R. Gao, N. Zhong, L. Tong, X. Kou, W. Huang, H. Yang, S. Huang, J. Wu, G. Chen and G. Ouyang, *Cell Rep. Phys. Sci.*, 2022, **3**, 101153.
14. C. Zhong, C. Hu, D. Ouyang, A. Dan, Y. Zhong, Z. Cai and Z. Lin, *Chem. Eng. J.*, 2023, **477**, 146979.
15. S. Hudson, J. Cooney and E. Magner, *Angew. Chem. Int. Ed.*, 2008, **47**, 8582–8594.
16. A. Kumar, G. D. Park, S. K. S. Patel, S. Kondaveeti, S. Otari, M. Z. Anwar, V. C. Kalia, Y. Singh, S. C. Kim, B.-K. Cho, J.-H. Sohn, D. R. Kim, Y. C. Kang and J.-K. Lee, *Chem. Eng. J.*, 2019, **359**, 1252–1264.
17. H. Patel, D. Rawtani and Y. K. Agrawal, *Trends Food Sci. Technol.*, 2019, **85**, 78–91.
18. M. Feng, Z. Niu, C. Xing, Y. Jin, X. Feng, Y. Zhang and B. Wang, *Angew. Chem. Int. Ed.*, 2023, **62**, e202306621.
19. D. I. Fried, F. J. Brieler and M. Fröba, *ChemCatChem*, 2013, **5**, 862–884.
20. K. Thakur, C. Attri and A. Seth, *3 Biotech*, 2021, **11**, 427.
21. Z. Zhang, Y. Zheng, Z. Dou, M. Gu, M. Sun, J. Song, N. Gao, F. Cui, Y. Tian and G. Zhu, *ACS Cent. Sci.*, 2023, **9**, 488–493.
22. C. Xing, P. Mei, Z. Mu, B. Li, X. Feng, Y. Zhang and B. Wang, *Angew. Chem. Int. Ed.*, 2022, **61**, e202201378.
23. W. Huang, H. Yuan, H. Yang, X. Ma, S. Huang, H. Zhang, S. Huang, G. Chen and G. Ouyang, *Nat. Commun.*, 2023, **14**, 3644.
24. S. Huang, J. Li, Y. Lin, L. Tong, N. Zhong, A. Huang, X. Ma, S. Huang, W. Yi, Y. Shen, G. Chen and G. Ouyang, *J. Am. Chem. Soc.*, 2023, **146**, 1967–1976.
25. H. Liu, Y. Zhou, J. Guo, R. Feng, G. Hu, J. Pang, Y. Chen, O. Terasaki and X.-H. Bu, *J. Am. Chem. Soc.*, 2023, **145**, 23227–23237.
26. X. Wang, L. He, J. Sumner, S. Qian, Q. Zhang, H. O'Neill, Y. Mao, C. Chen, A. M. Al-Enizi, A. Nafady and S. Ma, *Nat. Commun.*, 2023, **14**, 973.
27. Y. Li, J. Liu, K. Zhang, L. Lei and Z. Lei, *Ind. Eng. Chem. Res.*, 2018, **57**, 559–567.
28. T. Li, Y. Wang, W. Liu, H. Fei, C. Guo and H. Wei, *Angew. Chem. Int. Ed.*, 2023, **62**, e202212438.
29. G. Chen, S. Huang, X. Kou, F. Zhu and G. Ouyang, *Angew. Chem. Int. Ed.*, 2020, **59**, 13947–13954.
30. J. Liang, J. Ruan, B. Njegic, A. Rawal, J. Scott, J. Xu, C. Boyer and K. Liang, *Angew. Chem. Int. Ed.*, 2023, **62**, e202303001.
31. C. Sicard, *Angew. Chem. Int. Ed.*, 2022, **62**, e202213405.
32. g. Li, X. Lv, W. Ji, Y. Zhou, Z. Lin, H. Cao and T. Tan, *J. Mater. Chem. A*, 2023, **11**, 7411–7418.
33. W. Huang, H. Yuan, H. Yang, L. Tong, R. Gao, X. Kou, J. Wang, X. Ma, S. Huang, F. Zhu, G. Chen and G. Ouyang, *JACS Au*, 2022, **2**, 2048–2058.
34. Y. Chen, F. Jimenez-Angeles, B. Qiao, M. D. Krzyaniak, F. Sha, S. Kato, X. Gong, C. T. Buru, Z. Chen, X. Zhang, N. C. Gianneschi, M. R. Wasielewski, M. Olvera de la Cruz and O. K. Farha, *J. Am. Chem. Soc.*, 2020, **142**, 18576–18582.
35. S. Huang, G. Chen and G. Ouyang, *Chem. Soc. Rev.*, 2022, **51**, 6824–6863.
36. Q. Yin, P. Zhao, R. J. Sa, G. C. Chen, J. Lu, T. F. Liu and R. Cao, *Angew. Chem. Int. Ed.*, 2018, **57**, 7691–7696.
37. F. Hu, C. Liu, M. Wu, J. Pang, F. Jiang, D. Yuan and M. Hong, *Angew. Chem. Int. Ed.*, 2017, **56**, 2101–2104. [10.1039/D4SC04619F](https://doi.org/10.1039/D4SC04619F)
38. Y. Zhou, C. Chen, R. Krishna, Z. Ji, D. Yuan and M. Wu, *Angew. Chem. Int. Ed.*, 2023, **62**, e202305041.
39. J. Jiang, B. Yu, S. Geng, H. Wang, W. Zhou, Z. Zhang and B. Chen, *Angew. Chem. Int. Ed.*, 2021, **60**, 25942–25948.
40. Y. Yang, L. Li, R. B. Lin, Y. Ye, Z. Yao, L. Yang, F. Xiang, S. Chen, Z. Zhang, S. Xiang and B. Chen, *Nat. Chem.*, 2021, **13**, 933–939.
41. Q. Zhu, L. Wei, C. Zhao, H. Qu, B. Liu, T. Fellowes, S. Yang, A. Longcake, M. J. Hall, M. R. Probert, Y. Zhao, A. I. Cooper and M. A. Little, *J. Am. Chem. Soc.*, 2023, **145**, 23352–23360.
42. D. Yu, H. Zhang, J. Ren and X. Qu, *Chem. Soc. Rev.*, 2023, **52**, 7504–7523.
43. Y.-L. Lee, Y.-T. Chou, B.-K. Su, C.-c. Wu, C.-H. Wang, K.-H. Chang, J.-a. A. Ho and P.-T. Chou, *J. Am. Chem. Soc.*, 2022, **144**, 17249–17260.
44. X. Gao, Y. Wang, E. Wu, C. Wang, B. Li, Y. Zhou, B. Chen and P. Li, *Angew. Chem. Int. Ed.*, 2023, **62**, e202312393.
45. I. Hisaki, C. Xin, K. Takahashi and T. Nakamura, *Angew. Chem. Int. Ed.*, 2019, **58**, 11160–11170.
46. R.-B. Lin and B. Chen, *Chem*, 2022, **8**, 2114–2135.
47. H. Li, C. Chen, Q. Li, X. J. Kong, Y. Liu, Z. Ji, S. Zou, M. Hong and M. Wu, *Angew. Chem. Int. Ed.*, 2024, **63**, e202401754.
48. K. Wang, Y. Li, L. H. Xie, X. Li and J. R. Li, *Chem. Soc. Rev.*, 2022, **51**, 6417–6441.
49. T. Wang, E. Lin, Y.-L. Peng, Y. Chen, P. Cheng and Z. Zhang, *Coord. Chem. Rev.*, 2020, **423**, 213485.
50. C. Kang, Z. Zhang, S. Kusaka, K. Negita, A. K. Usadi, D. C. Calabro, L. S. Baugh, Y. Wang, X. Zou, Z. Huang, R. Matsuda and D. Zhao, *Nat. Mater.*, 2023, **22**, 636–643.
51. X. Li, K. Zhang, G. Wang, Y. Yuan, G. Zhan, T. Ghosh, W. P. D. Wong, F. Chen, H.-S. Xu, U. Mirsaidov, K. Xie, J. Lin and K. P. Loh, *Nat. Synth.*, 2022, **1**, 382–392.
52. Y. Zhang, C. Xing, Z. Mu, Z. Niu, X. Feng, Y. Zhang and B. Wang, *J. Am. Chem. Soc.*, 2023, **145**, 13469–13475.
53. Y. Zhang, J. Phipps and S. Ma, *Nat. Catal.*, 2022, **5**, 973–974.
54. C. Gu, N. Hosono, J.-J. Zheng, Y. Sato, S. Kusaka, S. Sakaki and S. Kitagawa, *Science*, 2019, **363**, 387–391.
55. M. Li, H. Ren, F. Sun, Y. Tian, Y. Zhu, J. Li, X. Mu, J. Xu, F. Deng and G. Zhu, *Adv. Mater.*, 2018, **30**, 1804169.
56. K. Ma, P. Li, J. H. Xin, Y. Chen, Z. Chen, S. Goswami, X. Liu, S. Kato, H. Chen, X. Zhang, J. Bai, M. C. Wasson, R. R. Maldonado, R. Q. Snurr and O. K. Farha, *Cell Rep. Phys. Sci.*, 2020, **1**, 100024.
57. M. Zhang, J. Samanta, B. A. Atterberry, R. Staples, A. J. Rossini and C. Ke, *Angew. Chem. Int. Ed.*, 2022, **61**, e202214189.
58. C. E. Shields, X. Wang, T. Fellowes, R. Clowes, L. Chen, G. M. Day, A. G. Slater, J. W. Ward, M. A. Little and A. I. Cooper, *Angew. Chem. Int. Ed.*, 2023, **62**, e202303167.
59. P. Wied, F. Carraro, J. M. Bolivar, C. J. Doonan, P. Falcaro and B. Nidetzky, *Angew. Chem. Int. Ed.*, 2022, **61**, e202117345.
60. W. Liang, F. Carraro, M. B. Solomon, S. G. Bell, H. Amenitsch, C. J. Sumby, N. G. White, P. Falcaro and C. J. Doonan, *J. Am. Chem. Soc.*, 2019, **141**, 14298–14305.
61. J. D. Martin-Romera, E. Borrego-Marin, P. J. Jabalera-Ortiz, F. Carraro, P. Falcaro, E. Barea, F. J. Carmona and J. A. R. Navarro, *ACS Appl. Mater. Interfaces*, 2024, **16**, 9900–9907.
62. G. Chen, L. Tong, S. Huang, S. Huang, F. Zhu and G. Ouyang, *Nat. Commun.*, 2022, **13**, 4816.
63. X. Lian, Y. Fang, E. Joseph, Q. Wang, J. Li, S. Banerjee, C. Lollar, X. Wang and H.-C. Zhou, *Chem. Soc. Rev.*, 2017, **46**, 3386–3401.
64. S. Banerjee, C. T. Lollar, Z. Xiao, Y. Fang and H.-C. Zhou, *Trends Chem.*, 2020, **2**, 467–479.



ARTICLE

65. G. G. Silkstone, C. E. Cooper, D. Svistunenko and M. T. Wilson, *J. Am. Chem. Soc.*, 2005, **127**, 92–99.
66. F. I. Rosell, J. C. Ferrer and A. Grant Mauk, *J. Am. Chem. Soc.*, 1998, **120**, 11234–11245.
67. Z. Tang, X. Li, L. Tong, H. Yang, J. Wu, X. Zhang, T. Song, S. Huang, F. Zhu, G. Chen and G. Ouyang, *Angew. Chem. Int. Ed.*, 2021, **60**, 23608–23613.
68. W.-H. Chen, M. Vázquez-González, A. Zoabi, R. Abu-Reziq and I. Willner, *Nat. Catal.*, 2018, **1**, 689–695.



The data supporting this article have been included as part of the Supplementary Information.

Crystallographic data for HOF-PTBA has been deposited at the CCDC under accession number of 2351559 and can be obtained from CCDC website.

